The Astrophysical Journal, 884:160 (9pp), 2019 October 20 https://doi.org/10.3847/1538-4357/ab41f5

Flaring Activity of Proxima Centauri from *TESS* Observations: Quasiperiodic Oscillations during Flare Decay and Inferences on the Habitability of Proxima b

Krisztián Vida[1], Katalin Oláh[1], Zsolt Kővári[1], Lidia van Driel-Gesztelyi[1,2,3], Attila Moór[1], and András Pál[1]
[1] Konkoly Observatory, MTA CSFK, H-1121 Budapest, Konkoly Thege M. út 15-17, Hungary; vidakris@konkoly.hu
[2] University College London, Mullard Space Science Laboratory, Holmbury St. Mary, Dorking, Surrey, RH5 6NT, UK
[3] LESIA, Observatoire de Paris, Université PSL, CNRS, Sorbonne Université, Université de Paris, 5 place Jules Janssen, F-92195 Meudon, France
Received 2019 July 29; revised 2019 August 26; accepted 2019 September 4; published 2019 October 22

Abstract

We analyze the light curve of the M5.5 dwarf Proxima Centauri obtained by the *Transiting Exoplanet Survey Satellite* (*TESS*) in Sectors 11 and 12. In the ≈50 day long light curve we identified and analyzed 72 flare events. The flare rate was 1.49 events per day; in total, 7.2% of the observing time was classified as flaring. The estimated flare energies were on the order of 10^{30}–10^{32} erg in the *TESS* passband (≈4.8× higher in bolometric energies, but on the same order of magnitude). Most of the eruptions appeared in groups. Two events showed quasiperiodic oscillations during their decay phase with a timescale of a few hours, which could be caused by quasiperiodic motions of the emitting plasma or oscillatory reconnection. From the cumulative flare frequency distribution we estimate that superflares with energy output of 10^{33} erg are expected to occur three times per year, while magnitude larger events (with 10^{34} erg) can occur every second year. This reduces the chances of habitability of Proxima Cen b, although earlier numerical models did not rule out the existence of liquid water on the planetary surface. We did not find any obvious signs of planetary transit in the light curve.

Unified Astronomy Thesaurus concepts: Stellar activity (1580); Stellar atmospheres (1584); Optical flares (1166); Stellar flares (1603); Low mass stars (2050); Late-type stars (909); M stars (985); Habitable zone (696); Planet hosting stars (1242); Habitable planets (695)

1. Introduction

At present, low-mass, cool M dwarfs are the prime targets of planet searches, since the habitable zone is much closer to the central object in cool stars than in the case of a solar-like star; thus, detecting a possibly habitable Earth-like planet is easier. Proxima Centauri, the nearest star to our Sun, has been the subject of such research (e.g., Benedict et al. 1999; Endl & Kürster 2008); recently, Anglada-Escudé et al. (2016) reported the discovery of Proxima b, a $1.27 M_\oplus$ planet orbiting within the habitable zone. The late spectral type (M5.5V) of the central star and the magnetic activity associated with it, however, could pose a threat to habitability.

The role of magnetic activity in planetary habitability is a currently actively studied field of research (see Scalo et al. 2007; Tarter et al. 2007; Seager & Deming 2010, and references therein). Flares, coronal mass ejections, and associated high-energy radiation and particles can have a serious impact on the environment by gradually evaporating planetary atmospheres (Khodachenko et al. 2007; Yelle et al. 2008; Chadney et al. 2017). A recent study of Vida et al. (2019), however, suggests that radiation effects would play the main role compared to coronal mass ejections in exoplanetary atmosphere evolution. Such frequent, high-energy events could cause the planetary atmospheres to be continuously altered, which is disadvantageous for hosting life (see Vida et al. 2017; Roettenbacher & Kane 2017 and references therein); however, a strong enough planetary magnetic field could provide some protection from these harmful effects (Vidotto et al. 2013).

Proxima Centauri is one of the few currently known ultracool objects that host an Earth-mass planet in its habitable zone, alongside the TRAPPIST-1 system (Gillon et al. 2017), Teegarden's star (Zechmeister et al. 2019), and the recently discovered GJ 1061 (Dreizler et al. 2019) and TOI-270 (Günther et al. 2019) systems, and is therefore an important proxy for understanding planet formation and evolution around ultracool dwarfs. Proxima Cen is the third distant member of the α Cen system consisting of two components of nearly solar mass A (G2V) and B (K1V), forming a visual binary provided all three stars were formed together, which is not yet fully settled (see Feng & Jones 2018). Stars A and B have rotational periods and magnetic activity cycle lengths resembling solar values: 17.5 days and >20 yr for component A, and 36.23 days and 8.9 yr for component B. Morel (2018) found an age of ≈6 Gyr for α Cen A and B from abundance indicators, which compares well to the possible age of Proxima Cen (about 5.1 Gyr) following from the rotation–age relation of Engle & Guinan (2018) with a rotational period of 83 days. The stellar system containing Proxima Cen is possibly older than the Sun. Proxima Centauri has a moderately strong magnetic field of ≈450–750 G (Reiners & Basri 2008). Its rotation period was estimated to be $P = 83.5$ days from *Hubble Space Telescope* data (Benedict et al. 1998) and $P = 82.5$ days using ASAS photometry (Kiraga & Stepien 2007). Despite being a slowly rotating, fully convective ultracool dwarf, it shows an activity cycle of ≈7 yr (see Wargelin et al. 2017 and references therein), although this would be expected for faster rotating stars of solar-like structure (see Vida et al. 2013; Wargelin et al. 2017 and references therein). Parameters of Proxima Centauri and its planet are summarized in Table 1.

The flaring activity of Proxima Centauri was detected in multiple wavelengths from the millimeter to the X-ray regime (Güdel et al. 2004; Fuhrmeister et al. 2011; MacGregor et al. 2018). Based on high-resolution optical spectra Pavlenko et al. (2017) concluded that the atmospheric structure of the star is rather complicated, consisting of a normal M5 dwarf photosphere, an extended hot envelope, and a hot stellar wind with a typical velocity of $V_r = 30\ \mathrm{km\ s^{-1}}$ that yields a minimum mass

Table 1
Parameters of the Proxima Centauri System

Parameters of Proxima Centauri		Reference
Mass	$0.120 \pm 0.003 M_\odot$	Ribas et al. (2017)
Radius	$0.146 \pm 0.007 R_\odot$	Ribas et al. (2017)
Luminosity	$0.00151 \pm 0.00008 L_\odot$	Ribas et al. (2017)
$T_{\rm eff}$	2980 ± 80 K	Ribas et al. (2017)
$\log g$	5.02 ± 0.18	Passegger et al. (2016)
[Fe/H]	-0.07 ± 0.14	Passegger et al. (2016)
Parallax	768.5 ± 0.2 mas	*Gaia* Collaboration (2018)
Age	≈6 Gyr	Morel (2018)
Magnetic field strength	450–750 G (3σ)	Reiners & Basri (2008)
Rotation period	≈83 days	Benedict et al. (1998); Kiraga & Stepien (2007)
Activity cycle length	≈7 yr	Wargelin et al. (2017)
Habitable zone range	≈0.0423–0.0816 au	Anglada-Escudé et al. (2016)
Habitable zone periods	≈9.1–24.5 days	Anglada-Escudé et al. (2016)
Parameters of Proxima Centauri b		
Orbital period	11.186 ± 0.001 days	Anglada-Escudé et al. (2016)
Semimajor axis, *a*	0.0485 ± 0.05 au	Anglada-Escudé et al. (2016)
Minimum mass	$1.27 \pm 0.19 M_\oplus$	Anglada-Escudé et al. (2016)
Equilibriumtemperature	230 ± 10 K	Anglada-Escudé et al. (2016)

loss of $\dot{M} = 1.8 \times 10^{-14} M_\odot$ per year. The chromosphere layers were suggested to be heated by flares (Pavlenko et al. 2019). Flare events were reported also using photometric observations: Davenport et al. (2016) analyzed *MOST* observations of 37.6 days, and found 66 flare events in white light with energies of 10^{29}–$10^{31.5}$ erg. In 2016 the Evryscope (Law et al. 2014) detected an eruption in the g' band that caused a ≈68× flux increase—a naked-eye superflare—that was estimated to have a bolometric flare energy of $10^{33.5}$ erg, and several other flares in the range of $10^{30.6}$–$10^{32.4}$ erg (Howard et al. 2018), while in 2017 another superflare was detected in the i' passband with at least 10% flux increase and an energy output of $>10^{33}$ erg (Kielkopf et al. 2019). In this paper, we analyze photometric observations of Proxima Centauri obtained by the *Transiting Exoplanet Survey Satellite* (*TESS*).

2. *TESS* Observations and Data Reduction

Proxima Centauri was observed by *TESS* in Sectors 11 and 12. Calibrated, short-cadence (2 min) data were downloaded from the MAST site.[4] We decided to use simple aperture photometry (SAP) data, since in the pre-search data conditioning (PDC) light curve instrumental and astrophysical signatures are removed to better isolate transits and eclipses, which is the primary scientific goal of the mission. The PDCSAP data show a somewhat lower scatter level, and they also remove a long-term trend from the light curve that could be compatible with the ≈80 day long rotation period. Since the length of the data set (53 days) is shorter than the rotation period, the validity of this trend cannot be safely confirmed; however, this does not influence our further analysis. Oscillations on hourly timescales are present in both data sets (see Section 4 for details and Figure 5 for a comparison of the two light curves).

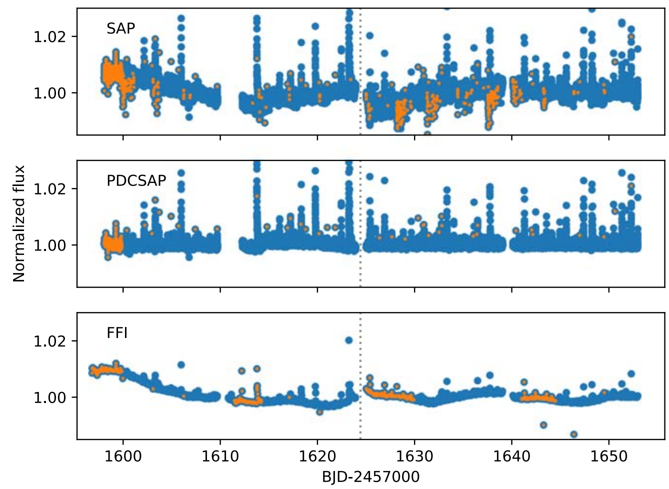

Figure 1. Comparison of the different photometric methods, from top to bottom: simple aperture photometry (SAP), pre-search data conditioning (PDCSAP), long-cadence data from full-frame images (FFI). Data points flagged as having quality problems are overplotted in orange. The dotted vertical line separates data from Sectors 11 and 12. The plots do not show the full range of the light curves.

From the light curve we excluded points where the quality flags indicated problems using a bit-wise AND operation with the binary mask 101010111111 as suggested by the *TESS* Data Product Overview.[5]

As a validity check, we also performed separate photometry on the 30 min cadence full-frame images (FFIs) to see if there were some serious issues with the automated pipeline. This photometry is based on differential imaging algorithms, implemented by various tasks of the FITSH package (Pál 2012). In this processing scheme, smaller, 96 × 96 pixel-sized image stamps are trimmed from the original FFI series, centered at the source. Columns with various artifacts were masked in order to avoid them in the derivation of the best-fit convolution transformation. The most prominent ill-calibrated block of CCD columns was associated with the blooming of the image of α Cen where charges bloomed into the smear region of the CCD; therefore, the automatic calibration procedure underestimated the pixel values at all of the affected columns. This convolution transformation accounts for all linear instrumental effects, including smear, spacecraft jitter, gradual offset due to differential velocity aberration, and background variations (due to stray light). Once these convolution kernel parameters are determined, differential and absolute fluxes are obtained by Equations (82) and (83) of Pál (2009), respectively. Similarly to the short-cadence data, FFIs are also flagged in a similar bit-mask scheme and photometric points corresponding to frames with unexpected flags are removed from further analysis. The resulting normalized light curves from the SAP, PDCSAP, and FFI data are compared in Figure 1. The long-term trend is visible in both the SAP and FFI light curves, suggesting that this is a physical phenomenon rather than an instrumental effect.

[4] https://mast.stsci.edu

[5] https://outerspace.stsci.edu/display/TESS/2.0+-+Data+Product+Overview

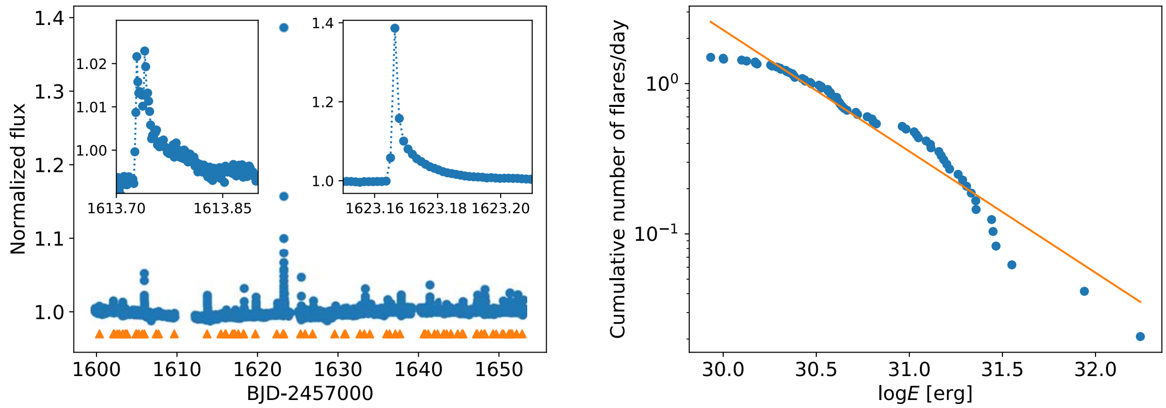

Figure 2. Left: *TESS* light curve (normalized SAP flux) of Proxima Centauri. The two insets show zoomed-in light curves of the largest flare events. Triangles mark the times of the identified flares. Right: cumulative flare frequency distribution fitted by a linear function.

Anglada-Escudé et al. (2016) predicted a transit depth of ≈0.5% (5 mmag) with a geometric transit probability of ≈1.5% and $P = 11.186$ days. A search by Feliz et al. (2019) ruled out transits with this period, and events shorter than 5 days with depths over 3 mmag. Although this is outside the main scope of this current paper, we did a quick period analysis to search for a possible transit, as an event of a few mmag depth should be easily noticeable (the precision of the FFI light curve is about 0.1 mmag); however, the predicted depth was not present in the data series.

3. Flare Detection and Flare Energies

Flare identification was done by visual inspection, in order to safely select also smaller events that automated algorithms tend to miss. To test the detection threshold of the visual inspection, we prepared a test data set with a scatter typical to the *TESS* data. To this artificial light curve 25 flares were added with random lognormal amplitude distribution (similar to the actual observations), with amplitudes ranging within a ≈0.5%–3% flux increase. This light curve was then analyzed in the same manner as the original *TESS* light curve. We found that the detection limit of our method is roughly a 0.001–0.002 increase in normalized intensity.

Of the 72 detected events, a sample is shown in Figure 2 (see also Figure 6 below). The light curves of the events were fit using the flare template of Davenport et al. (2014). The fits to the normalized light curves yielded amplitudes in the range of 0.0007–0.2 with a mean and median of 0.027 and 0.015, and full-width at half maximum values—describing roughly the timescale of the events—in the range of 0.0012–1.74 days, with mean and median values of 0.05 and 0.005, respectively. Note that the analytic models do not always fit well with the observations (especially in the case of small or complex events, or poorly sampled data), but these numbers can help to give an idea about the amplitude and timescale of the flares.

The flare energy estimation was done by integrating the normalized flare intensity during the event (see e.g., Vida & Roettenbacher 2018):

$$\varepsilon_f = \int_{t_1}^{t_2} \left(\frac{I_{0+f}(t)}{I_0} - 1 \right), \quad (1)$$

where t_1 and t_2 are the beginning and end times of the event, and I_{0+f} and I_0 are the intensities with and without a flare. This value gives the relative flare energy, or equivalent duration. To get the energy in the observed bandpass (E_f), we have to multiply this by the quiescent stellar luminosity ($L_\star$):

$$E_f = \varepsilon_f L_\star. \quad (2)$$

We estimated the quiescent luminosity using the spectrum of Proxima Centauri compiled by Ribas et al. (2017). This spectrum was convolved with the *TESS* response function and integrated over wavelength to obtain the observed quiescent luminosity, yielding $L_\star = 9.915 \times 10^{29}$ erg s^{-1} for the *TESS* bandpass.[6] The resulting flare energies are plotted in Figure 2 and summarized in Tables 2 and 3.

If dN is the number of flares in the energy range $E + dE$, $dN(E)$ can be written as

$$dN(E) \propto E^{-\alpha} dE \quad (3)$$

(see, e.g., Hawley et al. 2014 and references therein). The cumulative flare frequency distribution can be expressed in logarithmic form by integrating as

$$\log \nu = a + \beta \log E, \quad (4)$$

where ν is the cumulative frequency of the flares with given energy larger than E, with $\beta = 1 - \alpha$ (Gizis et al. 2017). To describe the characteristics of a flaring star, this distribution is usually fitted by a linear function, which yields the slope $1 - \alpha$. The best fit gives $\alpha = 1.81 \pm 0.03$ (see Figure 2). The given error is the formal error of the linear fit; the true uncertainty is probably a magnitude larger. Following Gizis et al. (2017), an alternative approach is to use an unbiased maximum likelihood estimator (corrected for the small sample size):

$$\alpha - 1 = (n - 2) \left[\sum_{i=1}^{n} \ln \frac{E_i}{E_{\min}} \right]^{-1}, \quad (5)$$

which yields $\alpha = 1.52$. This method has the advantage of being independent of the energy range chosen for the fit, which can significantly change the result. From *MOST* photometry Davenport et al. (2016) found a similar result of $\alpha = 1.68$.

According to Shibata et al. (2013) and Notsu et al. (2019) the bolometric energy released by a flare ($E_{\rm flare}$) and the area of the smallest spot that could produce such an event ($A_{\rm spot}$) are

[6] Available, e.g., at the *TESS* Science Support Center https://heasarc.gsfc.nasa.gov/docs/tess/the-tess-space-telescope.html.

Table 2
Flare Parameters for Sector 11 Data

№	Time [BJD-2,457,000]	Equivalent Duration (s)	Energy (erg)	Note
1	1600.3730	3.6778	3.647e+30	
2	1602.1231	11.2875	1.119e+31	
3	1602.2106	3.8165	3.784e+30	
4	1602.5675	1.2674	1.257e+30	
5	1602.8495	1.5051	1.492e+30	
6	1603.2675	20.4766	2.030e+31	double peaked
7	1603.5759	3.3961	3.367e+30	
8	1603.7037	2.3921	2.372e+30	
9	1603.7926	1.0143	1.006e+30	
10	1604.9051	3.3981	3.369e+30	
11	1605.0009	0.8642	8.569e+29	
12	1605.2648	3.7919	3.760e+30	double peaked
13	1605.6815	1.8447	1.829e+30	
14	1605.9482	29.4649	2.921e+31	
15	1607.4176	6.3550	6.301e+30	double peaked
16	1607.7038	13.1791	1.307e+31	
17	1609.6677	2.2111	2.192e+30	
18	1613.7400	87.8975	8.715e+31	triple peaked
19	1615.4594	2.3739	2.354e+30	
20	1616.0053	2.4455	2.425e+30	
21	1616.0636	10.7013	1.061e+31	double peaked
22	1616.8789	4.1078	4.073e+30	
23	1617.0789	5.9920	5.941e+30	
24	1617.1872	9.2374	9.159e+30	
25	1617.6178	2.7855	2.762e+30	
26	1618.2456	2.2871	2.268e+30	
27	1618.2928	27.9062	2.767e+31	
28	1619.7428	35.8418	3.554e+31	
29	1622.4053	9.6765	9.594e+30	
30	1623.1664	175.6592	1.742e+32	
31	1623.2748	14.9430	1.482e+31	

related as

$$E_{\rm flare} \approx f E_{\rm mag} \approx \frac{B^2}{8\pi} A_{\rm spot}^{3/2}, \tag{6}$$

where B is the magnetic field strength and f is the fraction of magnetic energy $E_{\rm mag}$ that can be released as a flare. To estimate the minimum areas for the flares observed by *TESS*, we converted the derived energies to bolometric ones. Following Günther et al. (2019), in this calculation, adopting 9000 K blackbody radiation model for flare emission, we obtained ∼4.8× larger bolometric energy release than that in the *TESS* band. By applying the above relation we then found that the observed flares come from an area $A_{\rm spot}$ at least ≈15%–30% of the projected visible stellar surface, using the bolometric energy of the largest observed flare as having a mean magnetic field strength B of 450–750 G, and assuming that the fraction of magnetic energy released as a flare (f) is 10% (see Shibata et al. 2013). This calculation overestimates the spot area, as the magnetic field strength in the active nest is higher than the measured global field. Following the method of

Table 3
Flare Parameters for Sector 12 Data

№	Time [BJD-2,457,000]	Equivalent Duration (s)	Energy (erg)	Note
32	1625.3539	15.4322	1.530e+31	
33	1625.9150	2.0581	2.041e+30	
34	1626.8428	13.0850	1.297e+31	
35	1629.5886	3.8677	3.835e+30	
36	1630.8136	2.6821	2.659e+30	
37	1630.9220	4.3070	4.270e+30	
38	1632.7275	16.0279	1.589e+31	
39	1633.2622	22.9272	2.273e+31	
40	1633.9580	4.1157	4.081e+30	
41	1636.0441	4.1674	4.132e+30	
42	1636.4108	12.4211	1.232e+31	
43	1637.1274	4.3895	4.352e+30	
44	1637.6927	28.4113	2.817e+31	
45	1640.6927	2.1842	2.166e+30	
46	1640.8704	1.5341	1.521e+30	
47	1641.2218	23.0312	2.284e+31	
48	1641.9954	1.0087	1.000e+30	
49	1642.3704	6.7074	6.650e+30	
50	1643.1204	1.3478	1.336e+30	
51	1643.1884	2.7649	2.741e+30	
52	1643.5037	5.2047	5.160e+30	
53	1644.0134	2.9587	2.934e+30	
54	1644.0398	2.9998	2.974e+30	
55	1644.8842	4.2421	4.206e+30	
56	1645.4092	2.4270	2.406e+30	
57	1645.5301	14.5296	1.441e+31	
58	1647.2078	4.6653	4.626e+30	
59	1647.3008	16.5996	1.646e+31	
60	1647.8119	2.0402	2.023e+30	
61	1648.1605	19.4783	1.931e+31	
62	1648.2494	11.0045	1.091e+31	
63	1649.2619	3.6956	3.664e+30	
64	1649.6494	3.2962	3.268e+30	
65	1650.4008	4.4968	4.459e+30	
66	1650.5563	1.9609	1.944e+30	
67	1651.2327	18.4329	1.828e+31	
68	1651.3702	1.4980	1.485e+30	
69	1651.5188	1.8163	1.801e+30	
70	1651.6368	6.4455	6.391e+30	
71	1652.1938	21.7023	2.152e+31	
72	1652.8799	5.3145	5.269e+30	

Howard et al. (2019) and Notsu et al. (2019) we can give another estimation of the spot area. First, we estimate the temperature of the starspots from the effective temperature:

$$\Delta T\,(T_{\rm star}) = T_{\rm star} - T_{\rm spot} = 3.58 \times 10^{-5} T_{\rm star}^2 + 0.249 T_{\rm star} - 808, \tag{7}$$

where $T_{\rm star}$ and $T_{\rm spot}$ are the temperatures of the unspotted and spotted photosphere. With normalized amplitude of the light variation caused by the spottedness ($\Delta F/F$) the spot area can be estimated based on the *TESS* light curve:

$$A_{\rm spot} = \frac{\Delta F}{F} A_{\rm star} \left[1 - \left(\frac{T_{\rm spot}}{T_{\rm star}}\right)^4\right]^{-1} \tag{8}$$

yielding a spot area of ≈4%. This result agrees well with that of Howard et al. (2019) (see Figure 3) plotting the most powerful

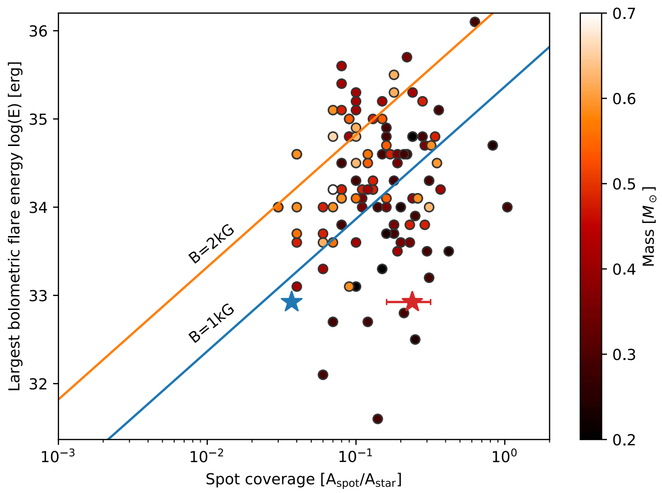

Figure 3. Flare energies as a function of spot area as a fraction of the projected visible surface. Red dots show data from the Evryscope project (Howard et al. 2019); blue and red stars show the largest observed flare on Proxima Cen in the *TESS* data using the method of Howard et al. (2019) and an estimation based on the measured global magnetic field, respectively. In the latter case (red star) the error bar corresponds to a 3σ uncertainty of the magnetic field (Reiners & Basri 2008). Solid lines show the minimum spot coverage needed to generate flares at the observed energies with 1 and 2kG field strength. The energy released by the event on Proxima Cen falls between that of solar and stellar flares (see Notsu et al. 2019).

flare from Table 2. The event on Proxima Cen falls between the rarely populated area of solar and stellar flares (see Notsu et al. 2019). We stress that the mass of Proxima Cen is lower than any of the stars in that sample (see Table 1), and falls between 0.2 and $0.7M_\odot$.

TESS was observing Proxima Centauri for a total of 1156 hours. During this time we detected 72 flare events, thus the total flare rate was 149 flares per day (0.062 flares per hour). In total, 7.2% of the total observing time was classified as flaring, Sector 11 data being somewhat less active than those of Sector 12. These values are similar to those found by Davenport et al. (2016) using *MOST* observation: they measured 8.1 flares per day in 2014 and 5.7 flares per day in 2015 (a total of 7.5% of the total observing time). We note that these numbers could be biased compared to a fast-rotating star; in that case, it is possible that a flare occurring on the opposite hemisphere can be detected as the star rotates within the timescale of the eruption, while in the case of Proxima Cen all the *TESS* observations do not cover even a whole rotation. According to Wargelin et al. (2017) the magnetic cycle length is ≈7 yr, with an activity minimum in 2012/2013. This means that the observation of the *MOST* satellite was done halfway to the activity maximum, while the *TESS* light curve was obtained close to the minimum. Interestingly, there is no significant change in the relative flaring activity across these epochs. After finishing its primary mission, the *TESS* could revisit Proxima Cen, and using those observations we could learn more about the long-term changes of the flaring activity of the object.

The flaring rate of Proxima Cen is similar to most of those observed on well-known flare stars, e.g., AB Dor: 0.5 (Jetsu et al. 1990) or EV Lac: 4.2 (Doyle 1987) flares per day, which have rotational periods from about 0.5 to a few days. Recently, Yang & Liu (2019) rigorously analyzed the K1 *Kepler* data for flaring stars. According to their Table 1, the highest flare frequencies—only for a few stars—are around 0.35 flares per day, and these stars have rotational periods of a few days. Looking at the slowest rotators, the dwarf flare star KIC 11027877 in Yang & Liu (2019), with the longest rotational period of 61.22 days, has a flare frequency of 0.02 flares per day, and another dwarf (KIC 9203794), with a rotation of 52.27 days, has 0.1 flares per day. Comparing Proxima Cen to these results, it seems that it has a very high flaring rate with an even slower rotational period, though the connection between the rotational rate (decreasing with age) and flaring activity would suggest otherwise (Davenport et al. 2019).

4. Observed Bumps during Flare Decay

The flares of Proxima Cen appear mostly in groups of two to many flares. From the 72 eruptions we find only a few definitely single events. The background of the multiplicity can be twofold: either the flares originate from the same activity source or, especially in case of very high flare frequency, are just coincidences (see Hawley et al. 2014 for details).

From the observed flares we find two events with a long decay phase. The first one lasts for over 1.5 days, and the second one for at least several hours (see the upper panels in Figures 4 and 5) and is a double event with a smaller secondary eruption. In the latter case the full decay is not seen, as the observations in Sector 11 finished before the star could return to quiescence. The observations of these two flares were cut after the faster decay phase and the remaining data from the slower decay were analyzed using the time–frequency method of short-term Fourier-transform (Kolláth & Oláh 2009). The lower panels in Figure 4 show the results of this time–frequency analysis. A pre-emphasis filter has been applied to suppress all the periodicities longer than 8.2 hr, since the amplitude of the decay itself is higher in the second case than the amplitudes of the bumps (for details see Kolláth & Oláh 2009, Section 2). For the first event (left plot in Figure 4) we find repeated bumps on a timescale of about 6.5 hr lasting for nearly a day with decreasing amplitude, and then damping until quiescence is reached (total analyzed data were about 1.85 days = 44.5 hr long). The second event is more energetic (see also Table 2), and its decrease shows clear repeating bumps on timescales of 2.7 and its double, 5.4 hr; the shorter period has higher amplitude at the beginning of the decrease, while the longer one is stronger at the end of the observations, when very probably the decay is still not finished (total analyzed data were about 0.6 days = 14 hr long).

Flare oscillations were observed previously on Proxima Cen in X-rays (Cho et al. 2016) and on several other stars in near-UV (Doyle et al. 2018). This latter paper also uses the time–frequency method (wavelet) to find the oscillation timescales. All these derived oscillation timescales for flare stars (including Proxima Cen) are on the order of a few to a few tens of seconds (between 20 and 120 s), i.e., much shorter than those we find for the bumps in the *TESS* wavelength range (roughly white light). It is likely that the origins of these features are different.

By analyzing *Kepler* light curves of different types of flaring stars from dwarfs to giants, Balona et al. (2015) and Pugh et al. (2016) found quasiperiodic bumps with characteristic periods of an hour (between 3 and 110 min). These values are the on same order as our result for the Proxima bumps. The characteristic timescales of the bumps can be very different on one star at different times, and the periods of the bumps do not show correlation of the physical parameters of the stars (see Pugh et al. 2016, their Figure 2). We note that Proxima Cen is very different from the stars observed by *Kepler* and studied by

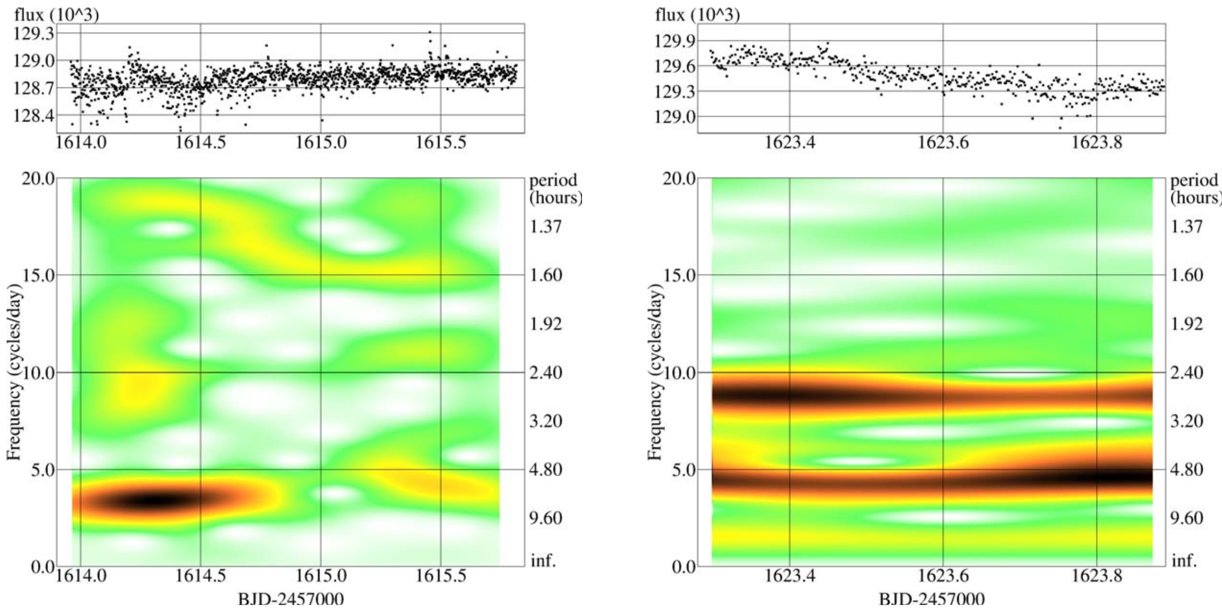

Figure 4. SAP fluxes after the two flares having post-flare bumps (top) and their short-term Fourier-transform (bottom). Left: timescale of the bumps is about 6.5 hr; right: repeating bumps of 2.7 and 5.4 hr. The black color marks the highest amplitude of the signal in the plot, while orange, yellow, and green show 50%, 20%, and 5% of that with continuous transition. See the text for more details.

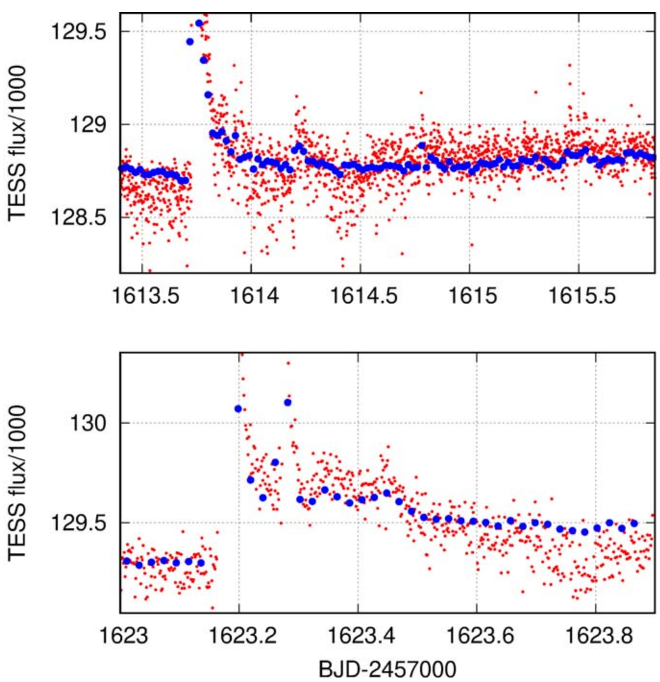

Figure 5. Comparison of the short-cadence simple aperture photometry data and long-cadence light curve obtained from photometry of full-frame images. Oscillations on an hourly timescale (see Section 4) are present in both data sets. Note that we do not show the full range of the light curve. The flux values of the short- and long-cadence data are shifted to match each other. The difference between them is about 3%, possibly due to the different reduction procedures applied.

Balona et al. (2015) and Pugh et al. (2016). Its rotational period (≈83 days) is about twice as long as that of KIC 2852961 (35.5 days; Pugh et al. 2016) and KIC 5952403 (45.28 days; Balona et al. 2015), which have bumps during their flare decrease; both of these are giants, while Proxima Cen is a low-mass dwarf star (Table 1).

The oscillatory pattern we find in the decay phase of these two long-duration flares on Proxima Centauri appears to be very similar to quasi-repetitive patterns with periods ranging from sub-second to several minutes observed in solar and stellar flares, which are called quasiperiodic pulsations (QPPs; e.g., Nakariakov et al. 2016). QPPs have been observed over the electromagnetic spectrum from radio through optical to X-rays indicating that they affect all layers of the solar or stellar atmosphere from the photosphere to the corona. Statistical studies seem to indicate that QPPs are not a rare phenomenon. Although not all flares show observable QPPs, larger flares tend to have such oscillatory patterns. For example, Simões et al. (2015) found that about 80% of X-class flares of the present solar cycle 24 had detectable QPPs.

Although there is still no consensus about the exact underlying physical mechanisms, there are several plausible candidates, which can be broadly divided into two categories (McLaughlin et al. 2018): (quasi-)periodic motions of the emitting plasma around an equilibrium, connected with the competition between inertia and an effective restoring force (incl. magnetohydrodynamic oscillations) and self-oscillatory mechanisms (e.g., load–unload models and relaxation processes in which a steady inflow of magnetic flux toward a reconnection site could result in repetitive magnetic reconnection (so-called magnetic dripping; Nakariakov et al. 2010). Another credible model in this category is oscillatory reconnection (McLaughlin et al. 2009; Murray et al. 2009; Threlfall et al. 2012) which—like other models that invoke magnetic reconnection—gives a natural explanation of the QPPs' multi-wavelength nature. In the oscillatory reconnection model there is competition between thermal-pressure and magnetic-pressure gradients, each successively overshooting the equilibrium created by the other. The resulting successive bursts of reconnection decrease in power as both pressure gradients decrease with time, allowing the system to approach an equilibrium state. In the model by Murray et al. (2009) oscillatory reconnection occurred between a newly emerging

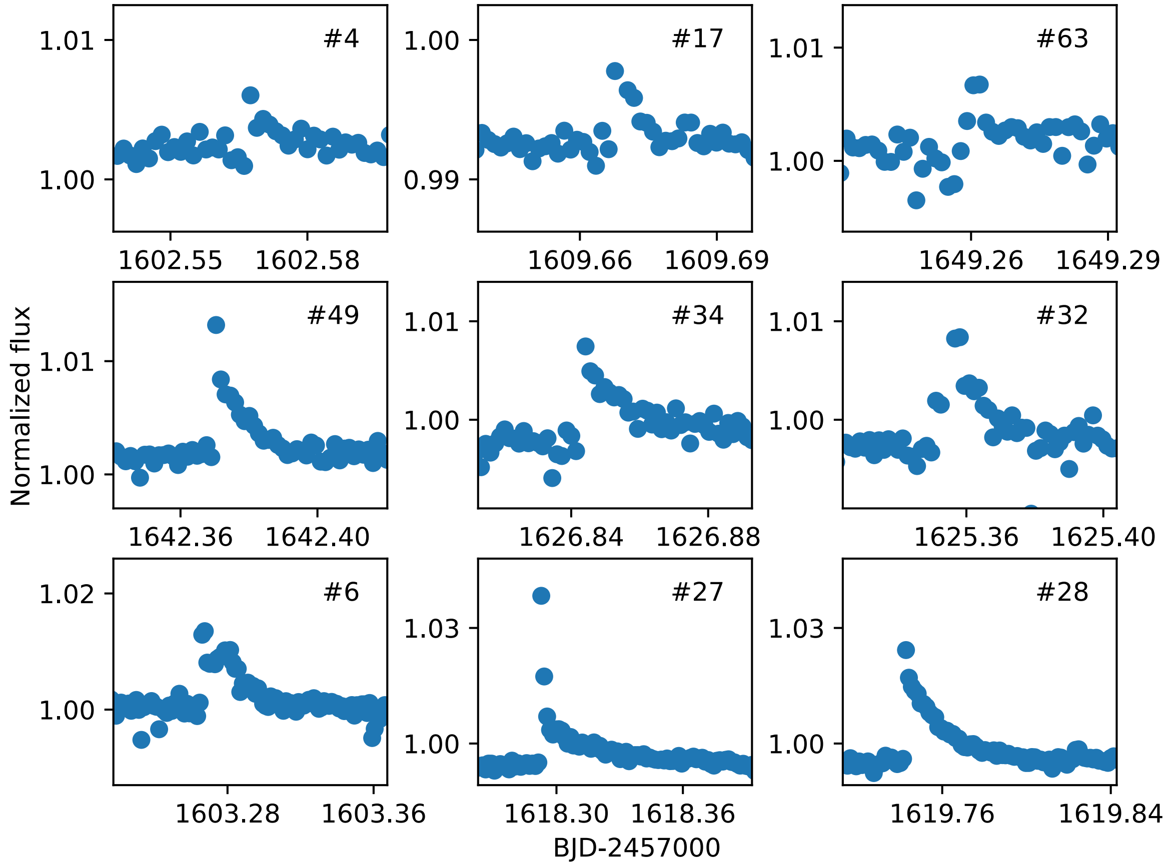

Figure 6. Selection of flares with different energy outputs. Numbers shown in the plots correspond to the event IDs in Tables 2 and 3.

magnetic flux and its locally open magnetic field environment. Emerging flux is one of the main flare triggers; the proposed mechanism appears plausible in the QPP-like oscillations we observe in the decay phase of two powerful flares on Proxima Centauri.

5. Implications for Habitability

Proxima Cen b is a $1.27M_{\oplus}$ planet, which orbits roughly at $1/20$ Sun–Earth distance to its host with an orbital period of roughly 11 days. The age of the system ($\approx$6 Gyr) would also make it a good target for the search for life. Numerical models suggest that the planet could have lost about an ocean's worth of water due to irradiation in the first 100–200 million years of its life (Ribas et al. 2016; Turbet et al. 2016), although the amount of initial water on the planet is unknown. After this period Proxima Cen b could either end up as a dry, atmosphereless planet by further loss of its atmospheric gases, or it could keep most of the atmosphere, preserving liquid water on the surface. In the latter scenario the authors concluded that liquid water may be present over the surface of the planet in the hemisphere facing the star, or in a tropical belt. According to these models, it cannot be ruled out that Proxima Cen b could be considered a viable candidate to be a habitable planet; this makes the effect of external factors, like flaring activity of the host star, even more interesting.

Unusually energetic flare events are often referred to as "superflares." The exact threshold for classifying an eruption as a superflare is somewhat arbitrary in the literature, but Kielkopf et al. (2019) suggested 10^{33} erg—roughly 10 times the energy output of the Carrington event on the Sun—as a reasonable value. Two such events have recently been observed on Proxima Cen: Howard et al. (2018) observed an eruption with a flux increase of $\approx$68 and a bolometric energy of $10^{33.5}$ erg, and Kielkopf et al. (2019) found another event with an estimated energy in the order of $\approx 10^{32}$–10^{33} erg in the Sloan i' band. According to Davenport et al. (2016), the frequency of such outbreaks is around eight times per year. From the *TESS* data we estimate roughly three superflares per year with an energy of 10^{33} erg, and about one event every two year with an energy output of 10^{34} erg (note that the *TESS* data were obtained roughly at the minimum of the magnetic activity cycle of Proxima Cen). These numbers are much higher than the estimated superflare frequency for G-type stars (Shibayama et al. 2013), roughly one per thousand years (10^{34}–10^{35} erg); therefore, such events could have a more serious effect on their surroundings than in the case of solar-like stars, especially since the planets orbit much closer to their hosts in late-type stars than in solar-like objects.

The effect of flares on exoplanetary habitability is strongly debated (see Lingam & Loeb 2017). UV radiation can modify, ionize, and even erode planetary atmospheres over time, leading to the photodissociation of important molecules such as water and ozone (Khodachenko et al. 2007; Yelle et al. 2008). On the other hand, planets orbiting M dwarfs may not receive enough UV flux for abiogenesis (i.e., the process by which life can arise from non-living simple organic compounds), which could be remedied by frequent flares (Ranjan et al. 2017). While Segura et al. (2010) showed that single, large flare events do not threat habitability around M dwarfs, strong, frequent flares can cause the planetary atmospheres to be continuously altered, making them less suitable for habitability (see Roettenbacher & Kane 2017; Vida et al. 2017, and references therein).

Currently there are only a few M-dwarf systems that are known to host Earth-like planets. These planetary systems are much tighter than our solar system—e.g., the planets around TRAPPIST-1 orbit between 0.01 and 0.06 au around their host, and the semimajor axis of Proxima Centauri b is 0.05 au (roughly at the distance of TRAPPIST-1 g). At these distances, both the radiation and the particle flux for such planets are much higher than for Earth—roughly 400 times higher for Proxima Centauri b compared to what the Earth receives when the Sun emits a flare of the same energy. Therefore, the activity of the central star can be more harmful to its habitable-zone planets in the case of M dwarfs. In two of the five such currently known systems—Proxima Centauri and TRAPPIST-1—the magnetic activity of the host seems to pose a serious threat to the habitability of their planets. Teegarden's star (Zechmeister et al. 2019), with an estimated age of >8 Gyr, has two known $1.3M_{\oplus}$ planets, and Wandel & Tal-Or (2019) found that surface liquid water could be present on both planets for a wide range of atmospheric properties, making these attractive targets for biosignature searches. The host star, however, is also known to flare (Zechmeister et al. 2019), but currently not much is known about its activity in detail. There are, however, two recently discovered systems that might provide a friendlier environment for life. GJ 1061 hosts a $1.5M_{\oplus}$ planet with the central star showing only occasional small flares (Dreizler et al. 2019), while TOI-270 is a nearby, quiet M-dwarf with a super-Earth ($1.25R_{\oplus}$) and two sub-Neptunes (2.42 and $2.13R_{\oplus}$). TOI-270 did not show any signs of rotational variability or flares during the photometric observations, and seems to have low activity according to Hα measurements as well (Günther et al. 2019). These possibly older systems (GJ 1061 is >7 Gyr old, TOI-270 has currently no age estimation) could be good candidates for detailed habitability studies if the atmospheres of their planets could survive the early active phase of the host star, or if the planets could acquire a secondary atmosphere at later stages of their lives, e.g., due to late bombardment (Kral et al. 2018; Dencs & Regály 2019) or outgassing (Godolt et al. 2019).

6. Summary

1. In the 53 day long light curve of Proxima Cen obtained by *TESS* in Sectors 11 and 12 we found 72 flare events.
2. The flare rate was 149 events per day, with 7.2% of the data being marked as flaring. The flares had an energy output on the order of 10^{29}–10^{32} erg, originating from at least ≈4%–30% of the stellar surface.
3. A fit to the cumulative flare frequency distribution yields $\alpha = 1.81 \pm 0.03$, while a maximum likelihood estimator gives $\alpha = 1.52$, in good agreement with previous findings.
4. Most of the flares are multiple/complex events; two of the events showed quasiperiodic post-flare oscillations with a timescale of a few hours, probably caused by periodic motions of the emitting plasma or oscillatory reconnection.
5. Superflares (events with energy output over 10^{33} erg) are expected around three times per year, and flares a magnitude larger (with 10^{34} erg) every second year; this could reduce the chances of Proxima Cen b being habitable, as the planet is only 1/20 au from the host star, and the fluence of radiation and particles increases inversely proportional to the square of the (decreased) distance.
6. Long-term trends can be seen in both the short-cadence SAP and the long-cadence FFIs, compatible with the ≈83 day long rotation period measured earlier. Unfortunately the length of the data set does not allow us to safely confirm this period.
7. No obvious signs of planetary transits were detected in the light curve.

The authors would like to thank the anonymous referee for the helpful comments and suggestions that significantly improved the paper. K.V. is supported by the Bolyai János Research Scholarship of the Hungarian Academy of Sciences. L.v.D.G. is partially funded under STFC consolidated grant No. ST/S000240/1. The authors thank the financial support from the National Research, Development and Innovation Office (NKFIH) under grant NKFI-KH 130372. This paper includes data collected with the *TESS* mission, obtained from the MAST data archive at the Space Telescope Science Institute (STScI). Funding for the *TESS* mission is provided by the NASA Explorer Program. STScI is operated by the Association of Universities for Research in Astronomy, Inc., under NASA contract NAS 526555.

Facility: TESS.

ORCID iDs

Krisztián Vida https://orcid.org/0000-0002-6471-8607
Katalin Oláh https://orcid.org/0000-0003-3669-7201
Zsolt Kővári https://orcid.org/0000-0001-5160-307X

References

Anglada-Escudé, G., Amado, P. J., Barnes, J., et al. 2016, Natur, 536, 437
Balona, L. A., Broomhall, A.-M., Kosovichev, A., et al. 2015, MNRAS, 450, 956
Benedict, G. F., McArthur, B., Chappell, D. W., et al. 1999, AJ, 118, 1086
Benedict, G. F., McArthur, B., Nelan, E., et al. 1998, AJ, 116, 429
Chadney, J. M., Koskinen, T. T., Galand, M., et al. 2017, A&A, 608, A75
Cho, I.-H., Cho, K.-S., Nakariakov, V. M., et al. 2016, ApJ, 830, 110
Davenport, J. R. A., Covey, K. R., Clarke, R. W., et al. 2019, ApJ, 871, 241
Davenport, J. R. A., Hawley, S. L., Hebb, L., et al. 2014, ApJ, 797, 122
Davenport, J. R. A., Kipping, D. M., Sasselov, D., et al. 2016, ApJL, 829, L31
Dencs, Z., & Regály, Z. 2019, MNRAS, 487, 2191
Doyle, J. G. 1987, A&A, 177, 201
Doyle, J. G., Shetye, J., Antonova, A. E., et al. 2018, MNRAS, 475, 2842
Dreizler, S., V., S., Jeffers, E., et al. 2019, arXiv:1908.04717
Endl, M., & Kürster, M. 2008, A&A, 488, 1149
Engle, S. G., & Guinan, E. F. 2018, RNAAS, 2, 34
Feliz, D. L., Blank, D. L., Collins, K. A., et al. 2019, AJ, 157, 226
Feng, F., & Jones, H. R. A. 2018, MNRAS, 473, 3185
Fuhrmeister, B., Lalitha, S., Poppenhaeger, K., et al. 2011, A&A, 534, A133
Gaia Collaboration, Brown, A. G. A., Vallenari, A., et al. 2018, A&A, 616, A1
Gillon, M., Triaud, A. H. M. J., Demory, B.-O., et al. 2017, Natur, 542, 456
Gizis, J. E., Paudel, R. R., Mullan, D., et al. 2017, ApJ, 845, 33
Godolt, M., Tosi, N., Stracke, B., et al. 2019, A&A, 625, A12
Güdel, M., Audard, M., Reale, F., Skinner, S. L., & Linsky, J. L. 2004, A&A, 416, 713
Günther, M. N., Pozuelos, F. J., Dittmann, J. A., et al. 2019, NatAs, tmp, 420
Günther, M. N., Zhan, Z., Seager, S., et al. 2019, arXiv:1901.00443
Hawley, S. L., Davenport, J. R. A., Kowalski, A. F., et al. 2014, ApJ, 797, 121
Howard, W. S., Corbett, H., Law, N. M., et al. 2019, ApJ, 881, 9
Howard, W. S., Tilley, M. A., Corbett, H., et al. 2018, ApJL, 860, L30
Jetsu, L., Vilhu, O., & La Dous, C. 1990, A&AS, 85, 1127
Khodachenko, M. L., Ribas, I., Lammer, H., et al. 2007, AsBio, 7, 167
Kielkopf, J. F., Hart, R., Carter, B. D., & Marsden, S. C. 2019, MNRAS, 486, L31
Kiraga, M., & Stepien, K. 2007, AcA, 57, 149
Kolláth, Z., & Oláh, K. 2009, A&A, 501, 695

Kral, Q., Wyatt, M. C., Triaud, A. H. M. J., et al. 2018, MNRAS, 479, 2649
Law, N. M., Fors, O., Wulfken, P., et al. 2014, Proc. SPIE, 91450Z, 91450Z
Lingam, M., & Loeb, A. 2017, ApJ, 848, 41
MacGregor, M. A., Weinberger, A. J., Wilner, D. J., et al. 2018, ApJL, 855, L2
McLaughlin, J. A., De Moortel, I., Hood, A. W., et al. 2009, A&A, 493, 227
McLaughlin, J. A., Nakariakov, V. M., Dominique, M., et al. 2018, SSRv, 214, 45
Morel, T. 2018, A&A, 615, A172
Murray, M. J., van Driel-Gesztelyi, L., & Baker, D. 2009, A&A, 494, 329
Nakariakov, V. M., Inglis, A. R., Zimovets, I. V., et al. 2010, PPCF, 52, 124009
Nakariakov, V. M., Pilipenko, V., Heilig, B., et al. 2016, SSRv, 200, 75
Notsu, Y., Maehara, H., Honda, S., et al. 2019, ApJ, 876, 58
Pál, A. 2009, PhD thesis, Eötvös Loránd University, Budapest
Pál, A. 2012, MNRAS, 421, 1825
Passegger, V. M., Wende-von Berg, S., & Reiners, A. 2016, A&A, 587, A19
Pavlenko, Y., Suárez Mascareño, A., Rebolo, R., et al. 2017, A&A, 606, A49
Pavlenko, Y. V., Mascareno, A. S., Zapatero Osorio, M. R., et al. 2019, A&A, 626, A111
Pugh, C. E., Armstrong, D. J., Nakariakov, V. M., et al. 2016, MNRAS, 459, 3659
Ranjan, S., Wordsworth, R., & Sasselov, D. D. 2017, ApJ, 843, 110
Reiners, A., & Basri, G. 2008, A&A, 489, L45
Ribas, I., Bolmont, E., Selsis, F., et al. 2016, A&A, 596, A111
Ribas, I., Gregg, M. D., Boyajian, T. S., et al. 2017, A&A, 603, A58
Roettenbacher, R. M., & Kane, S. R. 2017, ApJ, 851, 77
Scalo, J., Kaltenegger, L., Segura, A. G., et al. 2007, AsBio, 7, 85
Seager, S., & Deming, D. 2010, ARA&A, 48, 631
Segura, A., Walkowicz, L. M., Meadows, V., et al. 2010, AsBio, 10, 751
Shibata, K., Isobe, H., Hillier, A., et al. 2013, PASJ, 65, 49
Shibayama, T., Maehara, H., Notsu, S., et al. 2013, ApJS, 209, 5
Simões, P. J. A., Hudson, H. S., & Fletcher, L. 2015, SoPh, 290, 3625
Tarter, J. C., Backus, P. R., Mancinelli, R. L., et al. 2007, AsBio, 7, 30
Threlfall, J., Parnell, C. E., De Moortel, I., et al. 2012, A&A, 544, A24
Turbet, M., Leconte, J., Selsis, F., et al. 2016, A&A, 596, A112
Vida, K., Kővári, Z., Pál, A., et al. 2017, ApJ, 841, 124
Vida, K., Kriskovics, L., & Oláh, K. 2013, AN, 334, 972
Vida, K., Leitzinger, M., Kriskovics, L., et al. 2019, A&A, 623, A49
Vida, K., & Roettenbacher, R. M. 2018, A&A, 616, A163
Vidotto, A. A., Jardine, M., Morin, J., et al. 2013, A&A, 557, A67
Wandel, A., & Tal-Or, L. 2019, ApJL, 880, L21
Wargelin, B. J., Saar, S. H., Pojmański, G., et al. 2017, MNRAS, 464, 3281
Yang, H., & Liu, J. 2019, ApJS, 241, 29
Yelle, R., Lammer, H., & Ip, W.-H. 2008, SSRv, 139, 437
Zechmeister, M., Dreizler, S., Ribas, I., et al. 2019, A&A, 627, A49